Quenching of high-p_T hadrons: Energy loss versus color transparency

B. Z. Kopeliovich,[1] J. Nemchik,[2,3] I. K. Potashnikova,[1] and Iván Schmidt[1]

[1]*Departamento de Física, Universidad Técnica Federico Santa María; and Instituto de estudios avanzados en Ciencias e Ingeniera; and Centro Científico-Tecnológico de Valparaíso; Casilla 110-V, Valparaíso, Chile*
[2]*Czech Technical University in Prague, FNSPE, Břehová 7, 11519 Prague, Czech Republic*
[3]*Institute of Experimental Physics SAS, Watsonova 47, 04001 Kosice, Slovakia*

High-p_T hadrons produced in hard collisions and detected inclusively bear peculiar features: (i) they originate from jets whose initial virtuality and energy are of the same order and (ii) such jets are rare and have a very biased energy sharing among the particles, namely the detected hadron carries the main fraction of the jet energy. The former feature leads to an extremely intensive gluon radiation and energy dissipation at the early stage of hadronization, either in vacuum or in a medium. As a result, a leading hadron must be produced on a short length scale. Evaluation within a model of perturbative fragmentation confirms the shortness of the production length. This result is at variance with the unjustified assumption of long production length, made within the popular energy-loss scenario. Thus, we conclude that the main reason of suppression of high-p_T hadrons in heavy-ion collisions is the controlled-by-color-transparency attenuation of a high-p_T dipole propagating through the hot medium. Adjusting a single parameter, the transport coefficient, we describe quite well the data from the Large Hadron Collider and the Relativistic Heavy Ion Collider for the suppression factor R_{AA} as function of p_T, collision energy, and centrality. We observe that the complementary effect of the initial-state interaction causes a flattening and even fall of R_{AA} at large p_T. The azimuthal anisotropy of hadron production, calculated with no further adjustment, also agrees well with data at different energies and centralities.

I. INTRODUCTION

A colored parton produced with a high momentum in a hard reaction hadronizes, forming a jet of hadrons. It is natural to expect that the production time of such a jet, averaged over jet configurations, rises with the jet energy due to the effect of Lorentz time dilation. Although the jet is detected at macroscopic distances from the collision point, its space-time development at the early stages of hadronization can be probed with nuclear targets [1].

In this paper we concentrate on the rare type of jets in which the main fraction of the jet momentum is carried by a single (leading) hadron. In some cases, like in semi-inclusive deep-inelastic scattering (SIDIS), such events can be selected explicitly, because the fractional light-cone momentum z_h of the detected hadron can be measured. In high-p_T single-hadron production processes the fractional hadron momentum is unobserved, but the convolution of the steeply falling jet momentum distribution with the fragmentation function picks up high values of z_h (see Sec. II D). Thus, inclusive high-p_T hadron production without observation of the whole jet implicitly selects an unusual type of jets with a very biased sharing of energy.

Another generic feature of such jets is an extremely high initial virtuality, which is of the same order as the jet energy. This leads to a very intensive gluon radiation and energy dissipation at the early stage of hadronization. In order to respect energy conservation in the production of a high-z_h hadron, the radiative dissipation of energy must be stopped by the production of a colorless hadronic configuration (QCD dipole or prehadron) on a short time or length (we use both terms interchangeably) scale. This is considered in detail in Sec. II, where the rate of radiative energy loss in vacuum is

calculated as a function of time. The production length l_p of a colorless dipole finalizing hadronization is calculated within a model of perturbative hadronization and found to be rather short. The important observation is a weak dependence of l_p on p_T, which might look counterintuitive, because the Lorentz factor is expected to stretch l_p at higher p_T. However, the rate of energy dissipation increases as well, and this works in the opposite direction, trying to shorten l_p.

Since a colorless dipole is created at a short time scale inside a dense medium, it has to survive through the medium in order to be detected. The evolution of the dipole in the medium and its attenuation is the subject of Sec. III. The key phenomenon controlling the dipole surviving probability is color transparency, which corresponds to the enhanced transparency of the medium for small-size dipoles [2]. We employ the relation between the dipole cross section and transport coefficient (broadening) found in Refs. [3–6]. Correspondingly, the observed magnitude of hadron attenuation can be used as a probe for the transport coefficient, which characterizes the medium density.

In Sec. IV we compare the calculated suppression factor R_{AA} with data, as function of p_T, collision energy, and centrality of the collision. This comparison involves only one fitted parameter, $\hat{q}_0$, which is the maximal transport coefficient of the medium created in a central collision of given nuclei, at a given energy. Otherwise, this parameter is universal for all observables. The shape of the p_T dependence of R_{AA} is found to be in good accord with the data. In particular, the observed rise of $R_{AA}(p_T)$ at LHC is easily and naturally explained by the color transparency effect, calculated within the rigorous quantum-mechanical description known as the path-integral technique.

Comparison with data results in the transport coefficient, which ranges from $\hat{q}_0 = 1.2$ GeV^2/fm at $\sqrt{s} = 62$ up to 2 GeV^2/fm at $\sqrt{s} = 2.76$ TeV for collisions of heavy nuclei, gold, and lead. These values of the transport coefficient are about twice as large as those that were found in Ref. [7] within a simplified model of dipole evolution. Nevertheless, they are an order of magnitude smaller than what was found in the analysis [8], based on the energy-loss scenario (see, e.g., Ref. [9]), which relies on the unjustified assumption of a long production length l_p. It is worth emphasizing that our approach, based on perturbative QCD, is irrelevant to data at $p_T \lesssim 6$ GeV, which are apparently dominated by hydrodynamics.

An additional effect related to initial-state interactions (ISI) of the colliding nuclei is described in Sec. IV B. The excitation of higher Fock states by multiple interactions leads to enhanced nuclear suppression of particle production with large x_L and/or x_T [10], where $x_L \equiv x_F = 2p_L/\sqrt{s}$ and $x_T = 2p_T/\sqrt{s}$. This effect can be seen in the p_T dependence of R_{AA} at the Relativistic Heavy Ion Collider (RHIC) energies $\sqrt{s} = 200$ and 62 GeV. Moreover, Large Hadron Collider (LHC) data at $\sqrt{s} = 2.76$ TeV indicate a leveling of the R_{AA} behavior at the maximal measured p_T, and we expect even a fall at $p_T \gtrsim 100$ GeV.

A complementary test of our approach is provided by data on azimuthal anisotropy of produced hadrons, as is described in Sec. IV C. In fact, we explain the measured difference between R_{AA} for in- and out-of-plane events and the asymmetry parameter $v_2(p_T)$, with no additional adjustment.

II. ENERGY CONSERVATION: HOW LONG DOES HADRONIZATION LAST?

One should discriminate between the observation of a jet initiated by a parton produced in a hard reaction [e.g., high-p_T processes or deep-inelastic scattering (DIS)] and the detection of only a single hadron produced inclusively with a large fractional light-cone momentum in a hard process at high energies. The latter process corresponds to a very rare jet configuration, where the main fraction z_h of the jet energy E is carried by a single hadron, while all other hadrons in the jet must share the smaller energy $(1 - z_h)E$. The deficit of energy imposes certain constraints on the space-time development of such a jet, which differs from an averaged jet. Our definition of the characteristic time scales is illustrated in Fig. 1.
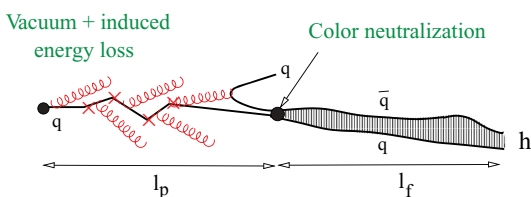
FIG. 1. (Color online) Space-time development of hadronization of a highly virtual quark producing a leading hadron, which carries the main fraction z_h of the initial quark light-cone momentum.

The quark regenerating its color field, which has been stripped off in a hard reaction, intensively radiates gluons and dissipates energy, either in vacuum or in a medium. Multiple interactions in the medium induce additional, usually less intensive, radiation. The loss of energy ceases at the moment, call production time t_p, when the quark picks up an antiquark neutralizing its color. The produced colorless dipole (also called prehadron) does not have either the wave function or mass of the hadron, but it takes the formation time t_f to develop both. The formation stage is described within the path-integral method in Sec. III B.

A. String model

The simple example of the consequences of energy conservation is the string (or color flux tube) model [11]. The usual expectation is that the higher is the energy of the produced hadron, the longer it takes to be produced, as follows from Lorentz time dilation. On the contrary, in Ref. [12] it was found that the production time of a hadron with energy $z_h E$ shrinks down to zero on reaching the kinematic bound of maximal energy E. Indeed, the quark that initiated a jet is losing its energy with the rate $dE/dt = -\kappa$, where $\kappa \approx 1$ GeV/fm is the string tension. The energy loss comes from the hadronization, which is developed as a series of string breaks by $\bar{q}q$ pairs tunneling from the vacuum [11].

Since the leading quark keeps losing energy, it can produce a hadron with energy $z_h E$ only within a certain time interval, restricted by energy conservation,

$$t_p \leqslant \frac{E}{\kappa}(1 - z_h). \qquad (1)$$

Such a shrinkage of the production time was explicitly confirmed in Monte Carlo models [13,14].

The string model is mentioned here only as an example of the constraints imposed on t_p by energy conservation. It should not be taken literally as a hadronization mechanism for hard reactions, where a highly virtual parton neutralizes its color perturbatively on a short time scale [15].

At this point we should specify our terminology in order to avoid further confusion. Indeed, different time scales are debated in the literature, including coherence time, formation time, and production time. What we call production time [in Eq. (1) and in what follows] is the time of color neutralization of the leading quark by an antiquark picked up from the string or generated perturbatively [15]. Notice that this is not yet the final hadron, which is characterized by both a specific wave function and mass. What is produced at the time scale t_p is a colorless $\bar{q}q$ dipole, having certain separation, but not mass, which we call conventionally prehadron. It takes the formation time to develop the wave function,

$$t_f = \frac{2E_h}{m_{h^*}^2 - m_h^2}, \qquad (2)$$

where $E_h = z_h E$; m_h and m_{h^*} are the masses of the hadron (we assume it to be the ground state) and the first radial excitation h^*. This time scale does not shrink at $z_h \to 1$ but keeps rising. It can be derived in the multichannel representation for

the diffractive scattering as the inverse minimal value of the longitudinal momentum transfer in the off-diagonal diffractive transitions between different states.

Equation (2) can also be understood in terms of the uncertainty principle. Namely, the produced $\bar{q}q$ dipole has a certain size and can be projected either to h or to h^*. According to the uncertainty principle, it takes the proper time $t_f^* = 1/(m_{h^*} - m_h)$ to resolve between these two levels. Applying the Lorentz boosting factor, we get (2).

Concerning the coherence time scale, this is a more general term, which means that quantum-mechanical interferences are important. Depending on the context and the employed theoretical tools, it might play a role in either the production time or the formation time.

B. Radiational energy loss

As a result of hard interaction characterized with the scale Q^2, the parton is produced with part of its color field stripped off, up to transverse frequencies $k_T \lesssim Q$. Hadronization of such a highly virtual quark cannot be described adequately in terms of the nonperturbative string model. Regeneration of the quark color field is associated with radiation of gluons, which take away a part of the quark energy and contribute to the formation of the jet. In fact, at high virtualities Q^2 this gluon radiation becomes the dominant source of energy loss in a vacuum.

One should strictly discriminate between vacuum and medium-induced energy loss. The former includes the lost energy, which goes into gluon radiation and/or into setting up the string field, in other words, into jet formation. The latter corresponds to the additional energy loss caused by the multiple interactions of the jet in the medium. The vacuum rate of energy loss usually significantly exceeds the medium-induced one. Here we concentrate on the study of the hadronization pattern in vacuum.

The time-dependent radiational energy loss can be calculated as follows [1,16,17]:

$$\Delta E_{\text{rad}}(t) = E \int_{\lambda^2}^{Q^2} dk^2 \int_0^1 dx\, x\, \frac{dn_g}{dx\, dk^2}\, \Theta\big(t - t_c^g\big), \quad (3)$$

where the coherence time for radiation of a gluon with fractional light-cone momentum x and transverse momentum k reads

$$t_c^g = \frac{2Ex(1-x)}{k^2 + x^2 m_q^2}. \quad (4)$$

The step function in Eq. (3) excludes from the integration those gluons which are still in coherence with the radiation source and did not materialize on mass shell during the time interval t. The soft cutoff λ in Eq. (3) is fixed at $\lambda = 0.7$ GeV. This choice is dictated by data (see in Refs. [18,19]), which indicates a rather large primordial transverse momentum of gluons.

The spectrum of radiated gluons in Eq. (3) has the form

$$\frac{dn_g}{dx\, dk^2} = \frac{2\alpha_s(k^2)}{3\pi\, x}\, \frac{k^2[1 + (1-x)^2]}{\big[k^2 + x^2 m_q^2\big]^2}, \quad (5)$$

where $\alpha_s(k^2)$ is the running QCD coupling.

The time dependence of radiational energy loss in vacuum exposes a nontrivial behavior [1,17]. During the time interval $t < (2E/Q^2)(1 - z_h)$, the energy loss rises linearly with time,

$$\Delta E_{\text{rad}}(t) = t\, \frac{2\alpha_s}{3\pi}\, (Q^2 - \Lambda^2). \quad (6)$$

However, at larger t, the rate of energy loss starts falling, $\Delta E_{\text{rad}}(t)$ is leveling off, and at $t > (2E/\Lambda^2)(1 - z_h)$ the gluon radiation completely ceases. The quark then loses energy only via nonperturbative mechanisms (strings).

Similarly to Eq. (1), the production time is restricted by energy conservation to

$$\Delta E(t_p) \approx E(1 - z_h). \quad (7)$$

Apparently, the increase of the energy-loss rate in Eq. (1), $\kappa \Rightarrow \kappa + |dE_{\text{rad}}/dt|$, caused by gluon radiation, can only shorten the production time.

C. Peculiar aspects of high-k_T jets

The solution of Eq. (7), the production time of a leading (pre-)hadron, depends on the jet energy and virtuality. In deep-inelastic scattering (DIS) these are two independent variables and usually $E^2 \gg Q^2$.

For a parton produced with high transverse momentum k_T normal to the collision axis in the center-of-mass frame, its energy is $E \approx k_T$. The hard scale for such a process is also imposed by the transverse momentum, i.e., $Q^2 = k_T^2$. Thus, a high-k_T jet is in a unique kinematic domain of extremely high virtuality, $Q^2 = E^2$, which cannot be accessed in DIS. This fact leads to a specific behavior of the production time for high-p_T hadrons, which differs from what is usually measured in SIDIS.

Indeed, we can trace the dependence of t_p on E and Q^2 using the approximate relation analogous to Eq. (1),

$$t_p \lesssim \frac{E}{\langle |dE/dt| \rangle}\, (1 - z_h). \quad (8)$$

If one increases the jet energy, keeping the virtuality Q^2 fixed, so $\langle |dE/dt| \rangle$ does not vary, the production time rises linearly with E and eventually exceeds the time of jet propagation through the medium. Indeed, the observed magnitude of nuclear suppression of leading hadrons in SIDIS decreases with energy and vanishes at jet energies $E \sim 100$ GeV [20]. However, at medium and low energies [21,22] the energy-loss scenario [23], which assumes a long production time, fails to describe the nuclear suppression observed in SIDIS at large z_h and vice versa if one keeps the energy E fixed, but increases the virtuality Q^2, the mean rate of energy loss in the denominator of (8) rises, and the production time shrinks.

Therefore, it is not obvious what will happen to t_p if both the energy and virtuality rise simultaneously, as it happens for high-k_T jets. In spite of the rising Lorentz factor, the jet virtuality $Q^2 = E^2$ rises as well and causes a dramatic enhancement of radiative energy loss, which may result in a shorter production time.

Equation (3) describes the time dependence of the energy radiated by a virtual quark. The total amount of radiational energy loss is given by the same equation without the Θ function,

$$\Delta E_{tot} = \frac{8\alpha_s}{3\pi} E \ln\left(\frac{E}{\lambda}\right), \qquad (9)$$

where we assumed $x \ll 1$ and fixed α_s for the sake of simplicity. Let us inverse the problem of the time dependence of energy loss [Eq. (3)] and ask: How long does it take for a highly virtual quark or gluon with $Q^2 = E^2$ to radiate a fraction,

$$\delta(t) = \frac{\Delta E(t)}{\Delta E_{tot}}, \qquad (10)$$

of the total radiated energy? Solving Eq. (3) one gets [24]

$$t(\delta) = \begin{cases} \delta \frac{4}{E} \ln\left(\frac{E}{\lambda}\right) & \text{if } \delta < 1/\ln\left(\frac{E^2}{\lambda^2}\right) \\ \frac{2}{\lambda e}\left(\frac{E}{\lambda}\right)^{2\delta-1} & \text{if } \delta > 1/\ln\left(\frac{E^2}{\lambda^2}\right) \end{cases}. \qquad (11)$$

From the second line of this equation we conclude that a high-k_T parton radiates half of the total energy loss during a very short time interval, $t(\delta = 1/2) = 2/(e\lambda) \approx 0.2$ fm. This interval is independent of energy. The δ dependence of the time interval $t(\delta)$ is illustrated in Fig. 2 for several jet energies.

This confirms that a high-k_T parton radiates the main fraction of the energy vacuum loss at the early stages of hadronization on very short time intervals. Notice that inclusion of nonperturbative mechanisms of energy loss should lead to even faster dissipation of energy. Thus, we conclude that the fast degradation of energy of a highly virtual parton makes impossible the production of leading (pre-)hadrons on a long time scale.

So far we have explored the time dependence of radiation with no constraints on the radiation process. However, detection of a hadron carrying a large fraction z_h of the initial parton energy essentially affects the energy-loss pattern due to energy conservation. The production of leading hadrons in such jets was studied in Ref. [25], where it was found to have the form

$$\frac{\partial D_{\pi/q}(z_h, Q^2)}{\partial t_p} \propto (1 - \tilde{z}_h) S(t_p, z_h). \qquad (12)$$

Here $Q^2 = k_T^2$, and the time-dependent fractional momentum $\tilde{z}_h(t)$, reads

$$\tilde{z}_h(t_p) = \left\langle\frac{z_h}{x}\right\rangle = z_h\left[1 + \frac{\Delta E(t_p)}{E}\right] + O[z_h(1 - z_h)^2]. \qquad (13)$$

The energy loss $\Delta E(t_p)$ includes both perturbative and nonperturbative (strings) sources of energy dissipation. The former is calculated with Eq. (3), in which an additional kinematical constraint is introduced: the energy of radiated gluons, $\omega = \alpha E + k^2/4\alpha E$, should not exceed the bound $\omega < (1 - z_h)E$. Such a ban for radiation of part of the gluon spectrum during the time interval $t < t_p$ leads to a suppression known as Sudakov factor $S(t_p, z_h)$, introduced in Eq. (12). It is defined as $S(t_p, z_h) = \exp[-\langle n_g(t_p, z_h)\rangle]$, where the mean number of gluons $\langle n_g(t_p, z_h)\rangle$ which have radiation time shorter than t_p, but cannot be radiated due to energy conservation, is calculated with the same gluon spectrum [Eq. (5)]. Examples for the Sudakov factor at different values of z_h are shown in Fig. 3 as functions of the production length $l_p = t_p$ and for jet energies $E = 10$ and 100 GeV.

We see that energy conservation vetoing part of the radiation spectrum results in the Sudakov suppression factor, which substantially reduces the production time Eq. (12). Now we are in a position to perform numerical calculations for the production time distribution function. Examples for the differential fragmentation function Eq. (12), at $Q^2 = E^2 = p_T^2/z_h^2$, are depicted in Fig. 4 as function of l_p.

Since the absolute value of the fragmentation function steeply varies with z_h, we renormalized it by adjusting to the same value at $l_p = 0$, and plot it in arbitrary units. As a test of the modeled differential fragmentation function Eq. (12),
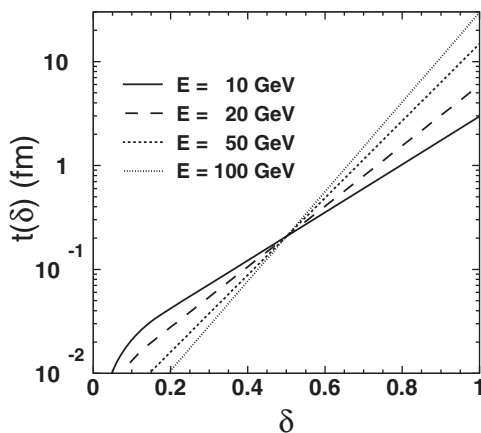
FIG. 2. The path length taken by a parton (quark or gluon) of energy E and virtuality $Q^2 = E^2$ to radiate a fraction $\delta = \Delta E(t)/\Delta E_{tot}$ of the total vacuum energy loss. The curves correspond to different jet energies, $E = 10, 20, 50,$ and 100 GeV.
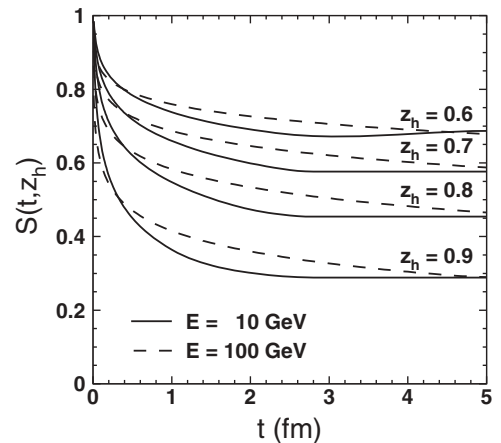
FIG. 3. Sudakov suppression factor caused by the ban for radiation of gluons with fractional energy higher than $1 - z_h$, during the time interval $t < t_p = l_p$. Calculations are done for jet energies, $E = Q = k_T = 10, 100$ GeV, and several fractional hadron momenta, $z_h = 0.6$–0.9.
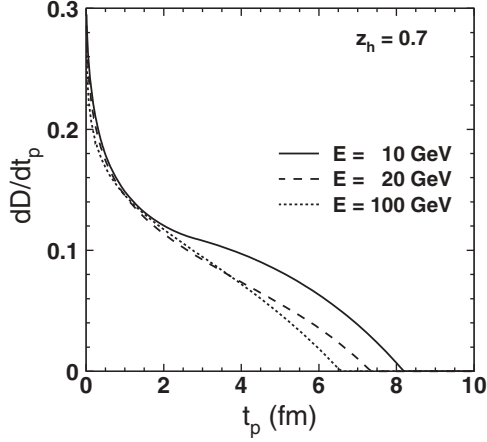
FIG. 4. The differential fragmentation function Eq. (12) (in arbitrary units) at $Q^2 = E^2$ as function of l_p for quark jets with energies $E = k_T = 10$, 20, and 100 GeV (from top to bottom) and $z_h = 0.7$.

we integrated it over t_p and compared with data. Our result reproduces fairly well [25] the phenomenological function $D_{\pi/q}(z_h, Q^2)$ [26] fitted to data at $z_h \gtrsim 0.5$. Correspondingly, we consider our calculated t_p distribution Eq. (12) to be accurate within this interval of z_h.

Eventually, using the distribution (12) we can calculate the mean production time,

$$\langle t_p(z_h, E) \rangle = \frac{1}{D_{\pi/q}(z_h, E^2)} \int dt_p \, t_p \frac{\partial D_{\pi/q}(z_h, E^2)}{\partial t_p}. \quad (14)$$

The results are presented in Fig. 5. Naturally, the production length for leading hadrons in jets initiated by gluons is shorter than for quarks, because the dissipation of energy in gluon jets is more intensive.

Notice that color neutralization, resulting in the production of a prehadron, also may be subject to coherence. This means that the amplitudes with different t_p can interfere, so one cannot identify with certainty the production moment
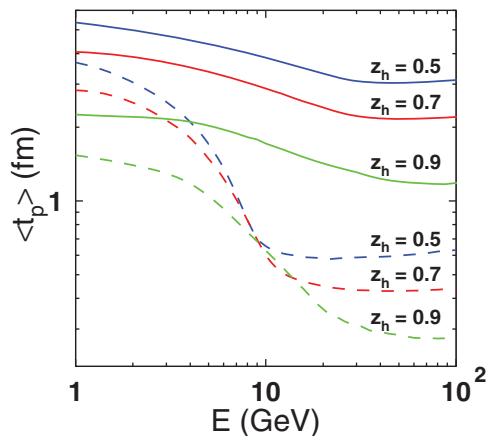
FIG. 5. (Color online) The mean production length as function of energy for quark (solid curves) and gluon (dashed curves) jets. In both cases, the curves are calculated at $z_h = 0.5$, 0.7, and 0.9 (from top to bottom).

t_p. One may be even unable to say whether the prehadron was created inside or outside the medium. Such a quantum-mechanical uncertainty was explicitly demonstrated in a SIDIS example [27], where the interference term in the production cross section was found to be 100% important and negative. However, in the case of a high-p_T jet, the starting virtuality is so high, and the dissipation of energy so intensive, that every amplitude is constrained to have a short t_p. Therefore, in what follows, we rely on the probabilistic description of the space-time development illustrated in Fig. 1.

D. The mean value of z_h

As expected, the production time varies with z_h, which unfortunately cannot be measured in the process under consideration, but one can evaluate its mean value and then rely on it in further calculations. As was stressed above, inclusive production of hadrons with large transverse momentum enhances the large-z_h part of the fragmentation function $D(z_h, Q^2)$. This happens due to the steepness of the k_T spectrum of the produced partons, quarks, or gluons, which has to be convoluted with the fragmentation function. This convolution defines the mean fractional momentum $\langle z_h \rangle$.

First, we should check how well we can describe data in pp collisions. We employ the simple model proposed in Ref. [28], based on k_T factorization,

$$\frac{d\sigma_{pp}}{dy \, d^2 p_T} = K \sum_{i,j,k,l} \int dx_i dx_j d^2 k_{iT} d^2 k_{jT}$$
$$\times F_{i/p}(x_i, k_{iT}, Q^2) \, F_{j/p}(x_j, k_{jT}, Q^2)$$
$$\times \frac{d\sigma}{d\hat{t}}(ij \to kl) \frac{1}{\pi \, z_h} D_{h/k}(z_h, Q^2). \quad (15)$$

Here $d\sigma(ij \to kl)/d\hat{t}$ is the cross section of parton scattering; the kinematic variables and their relations can be found in Ref. [28]. Following Ref. [28] we assume a factorized form of the transverse-momentum distribution,

$$F_{i/p}(x, k_T, Q^2) = F_{i/p}(x, Q^2) \, g_p(k_T, Q^2), \quad (16)$$

where

$$g_p(k_T, Q^2) = \frac{1}{\pi \langle k_T^2(Q^2) \rangle} e^{-k_T^2 / \langle k_T^2(Q^2) \rangle}. \quad (17)$$

The scale dependence of $\langle k_T^2(Q^2) \rangle$ was parametrized in Ref. [28] as $\langle k_T^2 \rangle_N(Q^2) = 1.2 \, \text{GeV}^2 + 0.2 \alpha_s(Q^2) Q^2$, with parameters adjusted to next-to-leading order calculations. We use the phenomenological parton distribution functions (PDF) $F_{i/p}(x, Q^2)$ from MSTW08 leading order (LO) [29]. For the fragmentation function $D_{h/k}(z_h, Q^2)$ we rely on the LO parametrization given in Ref. [30].

The results of the differential invariant cross-section calculations Eq. (15) are compared with data at $\sqrt{s} = 200 \, \text{GeV}$ [31] and 7 TeV [32] in Fig. 6. We see that the employed model reproduces quite well the shape of the measured cross section up to the maximal available momenta. The absolute normalization (not important for us) is regularized by the K factor in (15), which we found to be $k \approx 1$–1.5 depending on the energy.
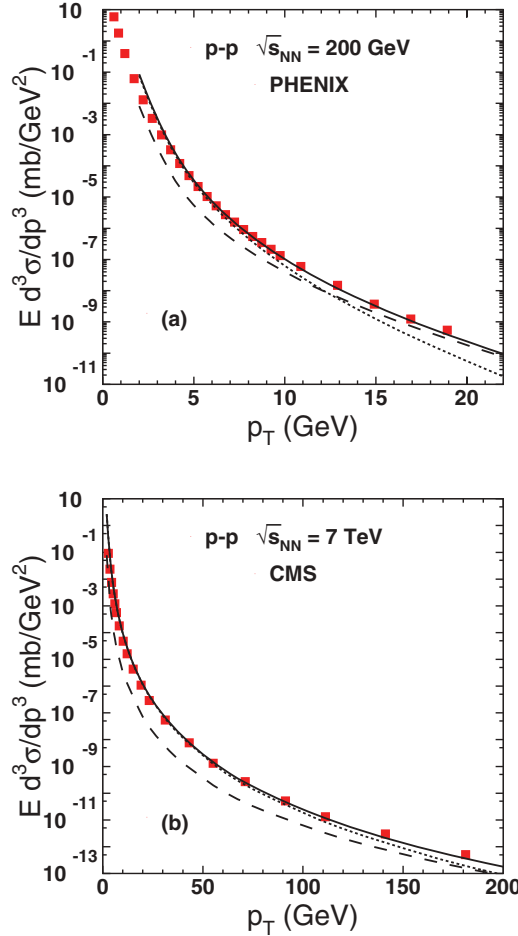
FIG. 6. (Color online) p_T dependence of pion production in pp collisions at $\sqrt{s} = 200$ GeV (a) and charged hadron production at 7 TeV (b). The contributions of quark and gluon jets are shown by dashed and dotted curves, respectively. Data points are from the PHENIX [31] and CMS [32] experiments.

Note that while at the LHC energy the cross section is fully dominated by gluon jets, at $\sqrt{s} = 200$ GeV quarks are important and even dominate towards the upper end of the available range of p_T. Eventually, we can average the fractional hadron momentum z_h weighted with the convolution Eq. (15). The results are depicted in Fig. 7, separately for quark and gluon jets (upper and lower solid curves) and at different energies, $\sqrt{s} = 200$, 2760, and 7000 GeV. We see that the lower the collision energy, the larger the $\langle z_h \rangle$, especially at large p_T, because the parton k_T distribution gets steeper. In the energy range of the LHC, the magnitude of $\langle z_h \rangle$ practically saturates as function of $\sqrt{s}$ and p_T.

Such a large value of the fractional jet energy carried by a single inclusively detected high-p_T hadron (without observation of the whole jet) makes its space-time development differ markedly from an usual high-p_T jet, when the whole jet is reconstructed. In the latter case, if no special selection is made, the mean fractional momenta of hadrons are very small. Correspondingly, energy conservation does not impose any severe constraints on the hadronization time scale, which rises with p_T and may be long.

III. ATTENUATION OF LEADING HADRONS IN A DENSE MEDIUM

In previous sections we found that in rare events, in which the produced hadron carries the main fraction z_h of the initial parton light-cone momentum, the intensive gluon radiation and energy dissipation in vacuum by a highly virtual parton produced with high k_T does not leave much time for the hadronization process. Particularly, such rare events are selected by detecting a hadron with large p_T. Figure 7 shows that the detected hadron carries, on average, more than half of the jet momentum. In order to respect energy conservation, the intensive dissipation of energy by the parton should be stopped promptly by color neutralization, i.e., production of a colorless prehadron, otherwise the leading parton, which lost too much energy, will be unable to produce a hadron with large z_h. Other possibilities for reduction of the vacuum energy loss by nonradiation of gluons are strongly Sudakov suppressed. As a result, the time scale for production of a colorless dipole is rather short and does not rise with p_T, as is depicted in Fig. 5.

If this process occurs not in vacuum, but in a dense medium, multiple interactions of the parton generate more energy loss, which makes the production time even shorter. The further interactions of the dipole in the medium are mostly inelastic color exchange collisions. Indeed, the cross section of inelastic interactions is proportional to the dipole separation squared, r_T^2, while the elastic scattering cross section is $\propto r_T^4$, which is negligibly small. So any inelastic interaction of the colorless dipole with color exchange will resume the gluon radiation and dissipation of energy. Of course, color neutralization may happen again via creation of a new dipole, but such a reincarnation of the prehadron will result in a substantial reduction of its momentum.

Thus, we should evaluate the survival probability W, i.e., the chance for a dipole to escape from the dense medium having no inelastic interaction on the way out. Apparently, this is subject to the effect of color transparency [2], i.e., the rate of attenuation of small-size dipoles vanishes quadratically
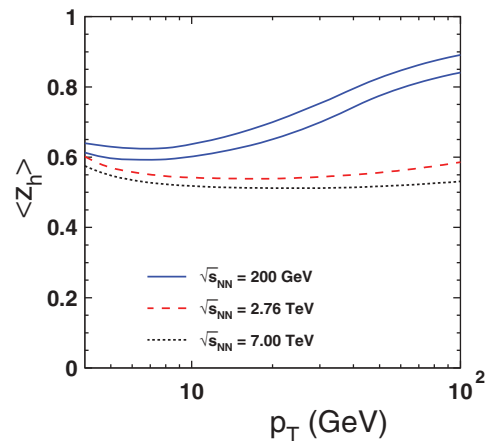
FIG. 7. (Color online) The mean fraction $\langle z_h \rangle$ of the jet energy carried by a hadron detected with transverse momentum p_T. The calculations are performed as described in the text for collision energies $\sqrt{s} = 200$, 2760, and 7000 GeV.

with the dipole transverse separation r,

$$\frac{dW}{dl}\bigg|_{r_T \to 0} = -\epsilon(l)\, r^2, \qquad (18)$$

where $\epsilon(l)$ characterizes the medium and varies with coordinates and time.

To avoid terminological confusions, notice that in high-p_T hadron production the momentum $\vec{p}_T$ is meant to be transverse to the collision axis. However, the "transverse" dipole separation is meant to be transverse relative to the vector $\vec{p}_T$.

It was found in Ref. [4] that a parton propagating through a nuclear medium experiences broadening, whose magnitude is controlled by the small-r behavior of the dipole-nucleon cross section. Thus, the broadening and attenuation rates in a medium turn out to be related as

$$\epsilon(l) = \tfrac{1}{2}\,\hat{q}(l). \qquad (19)$$

Here the broadening rate $\hat{q}(l) = \partial \Delta q^2/\partial l$ is usually called transport coefficient and used as a characteristic of the medium [33]. Notice that $\vec{q}$ is the transverse momentum of the parton relative to its initial direction. The transport coefficient is proportional to the medium density, which is function of impact parameter and time. In what follows, we rely on the popular, although poorly justified, model for $\hat{q}$, which is assumed to be proportional to the number of participants and gets diluted with time as $\rho(t) = 1/t$, due to the longitudinal expansion of the produced medium. Correspondingly, the transport coefficient depends on impact parameter and time (path length $l = t$) as [34]

$$\hat{q}(l, \vec{b}, \vec{\tau}) = \frac{\hat{q}_0\, l_0}{l}\, \frac{n_{\text{part}}(\vec{b}, \vec{\tau})}{n_{\text{part}}(0,0)}\, \Theta(l - l_0), \qquad (20)$$

where $\vec{b}$ is the impact parameter of nuclear collision, $\vec{\tau}$ is the impact parameter of the hard parton-parton collision relative to the center of one of the nuclei, $n_{\text{part}}(\vec{b}, \vec{\tau})$ is the number of participants, and $\hat{q}_0$ is the rate of broadening of a quark propagating in the maximal medium density produced at impact parameter $\tau = 0$ in central collisions ($b = 0$) at the time $t = t_0 = l_0$ after the collision. The corresponding transport coefficient for gluons should be 9/4 bigger. The equilibration time t_0 is model dependent. Our results are not very sensitive to it, and we fix it at $t_0 = l_0 = 0.5$ fm.

As far as the process of high-p_T hadron production is considered as a probe for the medium properties, we treat the transport coefficient $\hat{q}(l, \vec{b}, \vec{\tau})$ as an adjustable quantity. Once the shape of this function is fixed by the model Eq. (20), the only fitted parameter is the maximal value of the transport coefficient $\hat{q}_0$, which depends on atomic number A of the colliding nuclei.

A. Evolution and attenuation of a dipole: Heuristic description

Here we employ a simplified description of the time evolution, in terms of the mean dipole transverse separation. The dipole produced with a very small initial size $r \sim 1/k_T$ starts expanding with a speed given by the uncertainty relation

$dr/dt \propto 1/r$ [7,35,36]. Correspondingly, the l dependence of r is described by the following linear differential equation[1]:

$$\frac{dr}{dl} = \frac{1}{r(l)E_h\alpha(1-\alpha)}, \qquad (21)$$

where α and $1 - \alpha$ are the fractions of the dipole light-cone momentum carried by the quark and antiquark and $E_h = p_T$ is the energy of the dipole.

The solution of Eq. (21) reads

$$r^2(l) = \frac{2l}{\alpha(1-\alpha)p_T} + r_0^2, \qquad (22)$$

where r_0 is the initial dipole size. If it is small, $r_0 \sim 1/k_T$, its magnitude is quickly "forgotten." Indeed, the first term in (22) starts dominating at $l \gg 1/p_T$, and the value of the initial size r_0 is unimportant.

The mean value of $r^2(l)$ Eq. (22) can be used in Eq. (18) to evaluate the attenuation of a dipole, initially small and evolving its size in a medium characterized with a transport coefficient $\hat{q}$,

$$R_{AB}(\vec{b}, \vec{\tau}, p_T) = \int_0^{2\pi} \frac{d\phi}{2\pi} \exp\left[-\frac{4}{p_T} \int_L^\infty dl\, l\, \hat{q}(l, \vec{b}, \vec{\tau} + \vec{l}) \right]. \qquad (23)$$

This is the medium attenuation factor for a dipole produced in a hard internal NN collision at impact parameter $\vec{\tau}$ in a collision of nuclei A and B with impact parameter $\vec{b}$. The produced hadron is detected at azimuthal angle ϕ relative to $\vec{b}$, i.e., $\vec{l} \cdot \vec{b} = lb\cos\phi$. The bottom limit of l integration is $L = \max\{l_p, l_0\}$. The dependence of the transport coefficient on coordinates is given by Eq. (20). In (23) we fixed $\alpha = 1/2$, because the dipole distribution amplitude over $\vec{r}$ and α is projected to the hadron (pion) wave function, which has a maximum at $\alpha = 1/2$ [37]. Moreover, we rely on Berger's approximation [38], which fixes α at this value.

This simplified approach was employed in Ref. [7] and described quite well the first data from the ALICE experiment [39] for central collisions. Important observations made in Ref. [7] are (i) the value of the parameter $\hat{q}_0$ needed to explain the observed suppression is an order of magnitude smaller than the results of the data analysis [8], based on the energy-loss scenario. At the same time, it agrees well with the perturbative evaluation of $\hat{q}_0$ [33] and with the analysis [35,36] of data on suppression of J/Ψ produced in central gold-gold collisions at $\sqrt{s} = 200$ GeV. (ii) The observed rising p_T dependence of $R_{AA}(p_T)$ [39] is naturally explained by the effect of color transparency [Eq. (18)]. Namely the higher the dipole energy $E_h = p_T$ (in the medium rest frame), the higher the Lorentz dilation of the dipole size expansion and, therefore, the lower the absorption. This is why there is a factor $1/p_T$ in the exponent of Eq. (23).

As was commented above, this simplified heuristic model allows to easily understand the main features of the underlying dynamics. It also allows to speed up the calculations. However, it misses some details which may affect the result. In particular,

---

[1]Factor 2 was missed in Ref. [7].

Eq. (21) describes the expansion of the dipole in vacuum. However, in a medium, color filtering effects modify the path-length dependence of the mean dipole separation. Namely dipoles of large size are strongly absorbed, while small dipoles attenuate less. Correspondingly, the mean separation in a dipole propagating in a medium should be smaller than that given by the differential equation (21) for the dipole expansion in vacuum. Introducing an absorptive term, we arrive at a modified evolution equation,

$$\frac{dr^2}{dl} = \frac{2}{E_h \alpha(1-\alpha)} - r^4(l)\,\epsilon(l), \qquad (24)$$

where $\epsilon(l)$ is related by (19) to the transport coefficient. Apparently, such a modification results in a reduction of the mean dipole size, making the medium more transparent. Correspondingly, we should expect that the analysis of ALICE data, performed in Ref. [7], should have underestimated the medium density, i.e., the parameter $\hat{q}_0$. We will return to this problem in Sec. IV A.

Unfortunately, Eq. (24) has an analytic solution only if $\epsilon(l)$ is constant, which is not the case here. Then one should solve the equation numerically, so the simplicity of such a heuristic model is lost. In these circumstances, it is worth switching to the rigorous quantum-mechanical description of the evolution and attenuation of a dipole in an absorptive medium and employ the path-integral approach [44].

B. Path-integral technique

Evolution and attenuation of a $\bar{q}q$ dipole propagating through an absorptive medium, starting from the transverse $\bar{q}q$ separation $\vec{r}_1$ at a point with longitudinal coordinate l_1 and

evolving its size up to $\vec{r}_2$ at the point l_2, is given by a sum over all possible trajectories of q and $\bar{q}$. The resulting survival probability amplitude has the form of a light-cone Green function $G_{\bar{q}q}(l_1, \vec{r}_1; l_2, \vec{r}_2)$, which satisfies the two-dimensional Schrödinger equation [18,40–42],

$$\left[i\frac{d}{dl_2} - \frac{m_q^2 - \Delta_{r_2}}{2\,p_T\,\alpha\,(1-\alpha)} - V_{\bar{q}q}(l_2, \vec{r}_2) \right] G_{\bar{q}q}(l_1, \vec{r}_1; l_2, \vec{r}_2)$$
$$= i\delta(l_2 - l_1)\,\delta(\vec{r}_2 - \vec{r}_1), \qquad (25)$$

and the boundary conditions

$$G_{\bar{q}q}(l_1, \vec{r}_1; l_2, \vec{r}_2)|_{l_1=l_2} = \delta(\vec{r}_2 - \vec{r}_1);$$
$$G_{\bar{q}q}(l_1, \vec{r}_1; l_2, \vec{r}_2)|_{l_1>l_2} = 0. \qquad (26)$$

The second term in square brackets in (25) plays role of the kinetic energy in the Schrödinger equation, while the imaginary part of the light-cone potential $V_{\bar{q}q}(l_2, \vec{r}_2)$ in (25) is responsible for absorption in the medium. According to Eqs. (18) and (19),

$$\text{Im}\, V_{\bar{q}q}(l, \vec{r}) = -\tfrac{1}{4}\,\hat{q}(l)\,r^2. \qquad (27)$$

The real part of the potential describes the nonperturbative interaction between q and $\bar{q}$ in the dipole [18,43]. It is questionable, however, whether such a binding potential should be considered within a hot, possibly deconfined, medium. Therefore, we will treat the $\bar{q}q$ as free noninteracting partons, like in the previous Sec. III A. The real potential should not affect the dipole evolution much in the initial perturbative stage of development.

In the case of a constant medium density, $\hat{q}(l) = \hat{q} = \text{const}$, Eq. (25) allows an analytic solution [44],

$$G_{\bar{q}q}(l_1, \vec{r}_1; l_2, \vec{r}_2) = \frac{\gamma}{2\pi i \sin(\omega\Delta l)} \, \exp\left\{ \frac{i\,\gamma}{2\sin(\omega\Delta l)} \big[(r_1^2 + r_2^2)\cos(\omega\Delta l) - 2\vec{r}_1 \cdot \vec{r}_2 \big] \right\} \exp\left[-\frac{im_q^2 \Delta l}{2p_T\alpha(1-\alpha)} \right] \qquad (28)$$

where $\Delta l = l_2 - l_1$ and

$$\omega^2 = -\frac{i}{2}\frac{\hat{q}}{p_T\alpha(1-\alpha)}; \qquad \gamma^2 = -\frac{i}{2}\,p_T\alpha(1-\alpha)\hat{q}. \qquad (29)$$

It was demonstrated in Refs. [44,45] that in the general case of arbitrarily varying medium density the Green function still retains the oscillatory form,

$$G_{\bar{q}q}(l_1, \vec{r}_1; l_2, \vec{r}_2) = \Omega(l_1, l_2)\exp\left[-\frac{im_q^2 \Delta l}{2p_T\alpha(1-\alpha)} \right] \exp\left\{ \Upsilon_1(l_1, l_2)\, r_1^2 + \Upsilon_2(l_1, l_2)\, r_1^2 + \Upsilon_3(l_1, l_2)\vec{r}_1 \cdot \vec{r}_2 \right\}. \qquad (30)$$

All information about the dipole absorption rate varying along its trajectory, $\hat{q}(l)$, is contained in the coefficients Ω and Υ_i. They are calculated numerically by slicing the medium into layers, which are sufficiently thin to keep $\hat{q}$, given by (20), constant within each of them. One then can calculate the coefficients $\Omega(l_1, l_2)$ and $\Upsilon_i(l_1, l_2)$, employing the recurrence relations between subsequent layers, derived in Refs. [44,45].

As in the previous section, we rely on the Berger model [38], which assumes equal sharing of the pion light-cone momentum between q and $\bar{q}$, i.e., $\alpha = 1/2$. Since the Green function is projected into the pion light-cone wave function, we have to keep $\alpha = 1/2$ for the dipole as well.

Now we are in a position to write a rigorous quantum-mechanical extension of the simplified model (23), for the suppression factor $R_{AB}(\vec{b})$ of hadrons produced with high p_T in a hard process in a collision of nuclei A and B with relative impact

parameter b,

$$R_{AB}(\vec{b}, p_T) = \frac{\int d^2\tau\, T_A(\tau) T_B(\vec{b} - \vec{\tau}) \int_0^{2\pi} \frac{d\phi}{2\pi} \left| \int_0^1 d\alpha \int d^2r_1 d^2r_2\, \Psi_h^\dagger(\vec{r}_2, \alpha) G_{\bar{q}q}(l_1, \vec{r}_1; l_2, \vec{r}_2) \Psi_{\rm in}(\vec{r}_1, \alpha) \right|^2}{T_{AB}(b) \left| \int_0^1 d\alpha \int d^2r\, \Psi_h^\dagger(\vec{r}_2, \alpha) \Psi_{\rm in}(\vec{r}_1, \alpha) \right|^2}$$

$$= \frac{1}{T_{AB}(b) |\Psi_h(0)|^2} \int d^2\tau\, T_A(\tau) T_B(\vec{b} - \vec{\tau}) \int_0^{2\pi} d\phi \left| \int_0^\infty dr\, r\, \Psi_h(r) G_{\bar{q}q}(0, 0; l_{\rm max}, r) \right|^2, \qquad (31)$$

where $T_{AB} = \int d^2\tau\, T_A(b) T_B(\vec{b} - \vec{\tau})$, ϕ is the azimuthal angle of the dipole trajectory in impact parameter plane, relative to the impact vector $\vec{b}$ of the collision, and $l_{\rm max}$ is any distance, which should be much longer that the extent of the medium. Its particular length is unimportant, because the Green function in vacuum is just a phase. Note that all information about the dipole trajectory, including the ϕ, $\vec{\tau}$, and $\vec{b}$ dependencies, is contained in the Green function. In (31) we fixed $r_0 = 0$, because, according to the solution of Eq. (22), it does make a difference whether r_0 is as small as $1/k_T$ or zero. It is also worth noting that we start the evolution of the Green function $G_{\bar{q}q}(l_1, \vec{r}_1; l_2, \vec{r}_2)$ at $l_1 = 0$, i.e., at the point of the hard collision, but assume that the absorptive imaginary part of the potential of Eq. (25) is zero at $l < l_0$ [compare with (20)]. Although the dipole does not exist at $l < l_p$, the parton virtuality is steeply falling, governed by the same equation (21), and the dipole is produced at $l = l_p$ with an enlarged separation, the same as if it had started evolution at $t = 0$. We note that the mean production length $\langle l_p \rangle$ differs for quark and gluon jets, as is demonstrated in Fig. 5. Therefore, the numerator in (31) is calculated separately for quark and gluon jets and then summed with the weights given by Eq. (15).

During the short path from $l = l_0$ to $l = l_p$ (if $l_p > l_0$), the parton experiences multiple interactions, which induce extra radiation of gluons and additional loss of energy [33],

$$\Delta E = \frac{3\alpha_s}{4} \Theta(l_p - l_0) \int_{l_0}^{l_p} dl \int_{l_0}^{l} dl'\, \hat{q}(l'). \qquad (32)$$

Although this is a small correction, we included it in the calculations by making a proper shift of the variable z_h in the fragmentation function.

IV. COMPARISON WITH DATA

Numerous results of new precise measurements at RHIC and LHC have been released recently. They allow us to perform stringent tests of the contemporary models of in-medium hadronization.

A. Quenching of high-p_T hadrons

The comparison of $R_{AA}(b, p_T)$ calculated within the simple model described in Sec. III A, with data from the ALICE experiment [39] at $\sqrt{s} = 2.76$ TeV, was performed in Ref. [7]. While the absolute value of R_{AA} is adjustable, its rising p_T dependence originates from the reduction of the mean dipole size with p_T, in accordance with Eq. (22), and due to Lorentz dilation of the dipole size expansion. As a result, the medium becomes more transparent for more energetic dipoles

in accordance with the effect of color transparency (CT), which makes the medium more transparent for smaller dipoles. An analogous rising energy dependence of medium transparency was predicted and observed for virtual photoproduction of vector mesons on nuclei [46]. So it was concluded in Ref. [7] that CT is the source of the rising p_T dependence of R_{AA} observed in the ALICE experiment [39].

Encouraged by the success of the simple model, we perform here full calculations employing the path integral method, Eq. (31). The results for central (0–5%) lead-lead collisions at $\sqrt{s} = 2.76$ TeV are shown by the dashed curve in Fig. 8, compared with new data from the ALICE [47] and CMS [48,49] experiments, extended to higher values of p_T than those in Ref. [39].

The only free parameter, the maximal transport coefficient defined in Eq. (20), was adjusted to the data and fixed at $\hat{q}_0 = 2$ GeV^2/fm for all further calculations for lead-lead collisions at this energy. Notice that this value of $\hat{q}_0$ is about twice as large as that found in Ref. [7] within the simple model described above in Sec. III A. As we commented, this should be expected, since Eq. (21) is lacking the color filtering effect added in (24) or inherited from the Green function equation (25).

While our calculations describe well the data at high $p_T \gtrsim 6$ GeV, the region of smaller p_T is apparently dominated
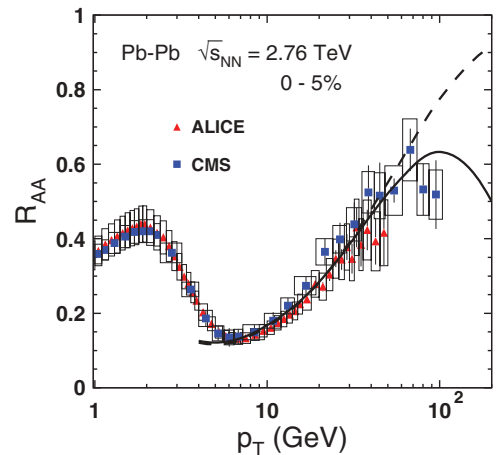
FIG. 8. (Color online) The suppression factor R_{AA} for central (0–5%) lead-lead collisions at $\sqrt{s} = 2.76$ TeV. The dashed line is calculated within the path-integral approach [Eq. (31)] with the space- and time-dependent transport coefficient Eq. (20), where the adjusted parameter $\hat{q}_0 = 2$ GeV^2/fm. The solid curve also includes the effects of initial state interactions in nuclear collisions [10,51], as is described in Sec. IV B. Data for R_{AA} are from the ALICE [47] and CMS [48,49] experiments.
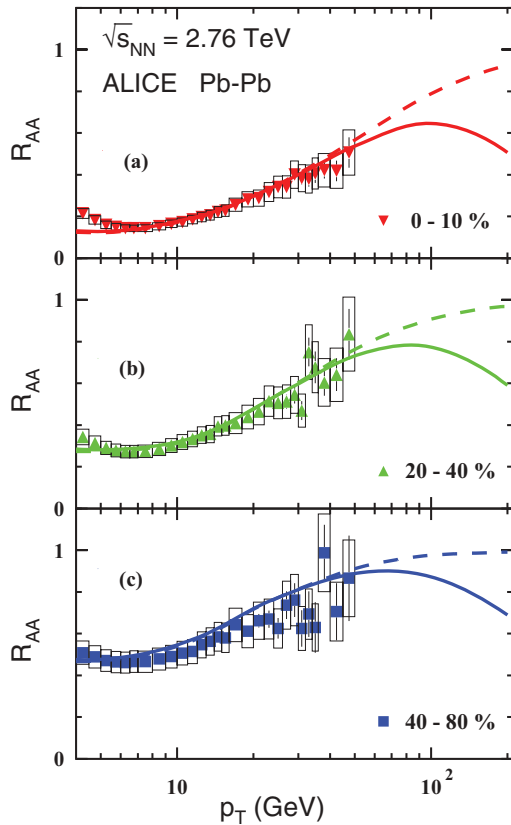
FIG. 9. (Color online) Centrality dependence of the suppression factor $R_{AA}(p_T, b)$ measured in the ALICE experiment [47]. The intervals of centrality are indicated in the plot. The meaning of the curves is the same as in Fig. 8.

by a thermal mechanisms of hadron production. We expect a sharp transition between the Hydro and pQCD regimes, as usually happens when the two regimes are characterized by exponential p_T dependencies with significantly different slopes. If the p_T dependence for produced hadrons parametrize as $\exp(-Bp_T)$, then the Hydro regime has slope $B = 1/T$, where the temperature $T = 0.3$ GeV was fitted to ALICE data. In the pQCD regime the p_T slope is $B \approx 1$ GeV^{-1} at $p_T \sim 6$ GeV. Thus, the Hydro-to-pQCD ratio varies as $\exp(-\Delta Bp_T)$. The transition region corresponds to the interval $\Delta p_T \sim 1/\Delta B = 0.4$ GeV. Notice that the blast-wave model for the high-p_T tail of the Hydro regime gives a somewhat smaller slope, $B = 2.2$ GeV^{-1} [50]. In this case, $\Delta p_T \sim 0.8$ GeV. We see that the transition region of p_T, where the two mechanisms are of the same order, is quite narrow. At smaller or larger p_T, one of the mechanisms is exponentially suppressed. The behavior of v_2 confirms this (see below): While Hydro predicts it monotonically rising with p_T, it abruptly falls down within the transition region of p_T.

The variation of the suppression factor $R_{AA}(p_T, b)$ with impact parameter of collision was also calculated with the Eq. (31). The results plotted by dashed curves are compared with data taken at different centralities of collision by the ALICE experiment [47] in Fig. 9 and by the CMS experiment [48,49] in Fig. 10. In all cases we observe good agreement.

B. Towards large x_T: New constraints from energy conservation

It was stressed in Refs. [10,51] that energy conservation may become an issue on approaching the kinematic bound of either large Feynman $x_L \equiv x_F = 2p_L/\sqrt{s}$ or transverse fractional momentum $x_T = 2p_T/\sqrt{s}$. Apparently, in such a kinematic domain, any initial state interactions (ISI) leading to energy dissipation should result in a suppressed production rate of particles with large $x_{L,T}$. Indeed, as it was stressed in Ref. [10], *every reaction* experimentally studied so far, with any particle (hadrons, Drell-Yan dileptons, charmonium, etc.) produced with large x_L, exhibits nuclear suppression. Observation of such a suppression in high x_T processes is more difficult, because the cross sections steeply fall with p_T, and available statistics may not be sufficient (see, however, Fig. 11). As in Ref. [51], we apply to high-p_T production exactly the same model developed in Refs. [10,52] for large x_L, and with the same parameters.

Since initial-state multiple collisions suppress the production rate of leading particles, we assume that every collision brings in a suppression factor $U(\xi)$ [10], where $\xi = \sqrt{x_L^2 + x_T^2}$. This factor $U(\xi)$ should cause a strong (for heavy nuclei) suppression at $\xi \to 1$, although at the same time some enhancement at small ξ due to the feed down from higher ξ. This is because energy conservation does not lead to disappearance (absorption) of particles but only to their redistribution in ξ.

Since at $\xi \to 1$ the kinematics of an inelastic collision corresponds to no particle production within the rapidity interval $\Delta y \sim -\ln(1 - \xi)$, the suppression factor $U(\xi)$ can also be treated as survival probability of a large rapidity gap, which is Sudakov suppressed. The mean number $\langle n_g(\Delta y) \rangle$ of gluons radiated in the rapidity interval Δy is related to the height of the plateau in the gluon spectrum, $\langle n_g(\Delta y) \rangle = \Delta y \, dn_g/dy$. The Sudakov factor then reads

$$U(\xi) = (1 - \xi)^{dn_g/dy}. \tag{33}$$
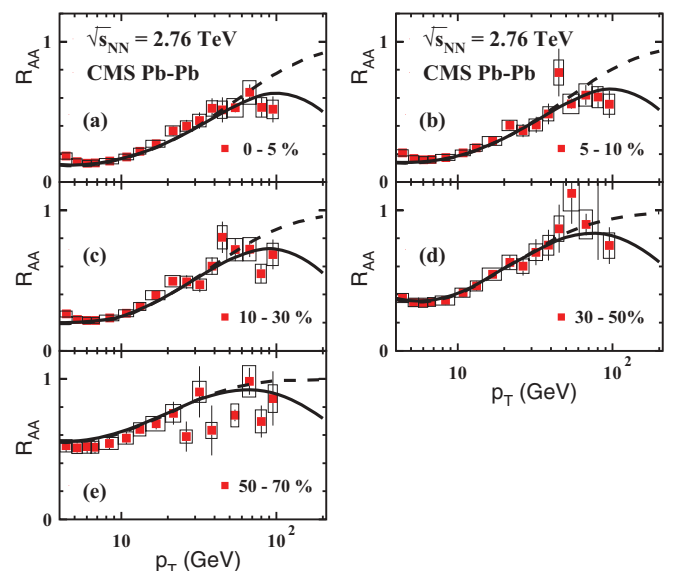
FIG. 10. (Color online) The same as in Fig. 9, with data from the CMS experiment [48,49].
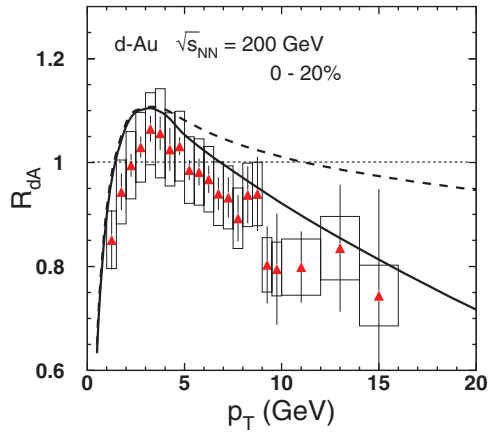
FIG. 11. (Color online) Nuclear attenuation factor $R_{dAu}(p_T)$ as function of p_T of π^0 mesons produced in central (0–20%) d-Au collisions at $\sqrt{s} = 200$ GeV and $\eta = 0$. The solid and dashed curves represent the model predictions calculated with and without the ISI corrections. Isotopic effect is included. The data are from the PHENIX experiment [56].

The height of the gluon plateau was estimated in Ref. [53] as

$$\frac{dn_g}{dy} = \frac{3\alpha_s}{\pi} \ln\left(\frac{m_\rho^2}{\Lambda_{\mathrm{QCD}}^2}\right). \tag{34}$$

The value of α_s was fitted in Ref. [53] at $\alpha_s = 0.45$, using data on pion multiplicity in e^+e^- annihilation. This leads with a good accuracy to $dn_g/dy \approx 1$, i.e., the Sudakov factor,

$$U(\xi) = 1 - \xi. \tag{35}$$

Although QCD factorization is expected to be broken by ISI in pA collisions at large ξ, we will rely on the effective factorization formula, Eq. (15), where we replace the proton parton distribution function by a nuclear modified one, $F_{i/p}(x_i, Q^2) \Rightarrow F_{i/p}^{(A)}(x_i, Q^2, b)$. In the case of nuclear collisions we do this modification for the bound nucleons in both nuclei. Relying on the suppression factor Eq. (35), and applying the AGK cutting rules [54] with the Glauber weight factors, one arrives at the ISI-modified parton distribution function of the proton in a pA collision at impact parameter b,

$$F_{i/p}^{(A)}(x_i, Q^2, b) = C\, F_{i/p}(x_i, Q^2)$$
$$\times \frac{[e^{-\xi\sigma_{\mathrm{eff}} T_A(b)} - e^{-\sigma_{\mathrm{eff}} T_A(b)}]}{(1-\xi)[1 - e^{-\sigma_{\mathrm{eff}} T_A(b)}]}. \tag{36}$$

Here σ_{eff} is the effective hadronic cross section controlling multiple interactions. It is reduced by Gribov inelastic shadowing, which makes the nuclear medium much more transparent. The effective cross section was evaluated in Refs. [10,55] at about $\sigma_{\mathrm{eff}} \approx 20$ mb. The normalization factor C in Eq. (36) is fixed by the Gottfried sum rule, because the number of valence quarks, dominating at large ξ, should be unchanged.

With the parton distribution functions Eq. (36) modified by ISI one achieves a good parameter-free description of available data at large x_L [10,51]. Moreover, these corrections may be important at large p_T, in particular in the RHIC energy range, where x_T reaches values of 0.2–0.3. Notice that the real values of x_T, essential for energy conservation, are significantly
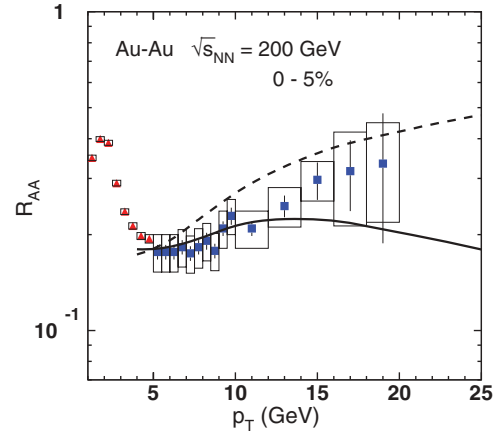
FIG. 12. (Color online) Nuclear attenuation factor $R_{AA}(p_T)$ for neutral pions produced in central gold-gold collisions at $\sqrt{s} = 200$ GeV. The solid and dashed line are calculated with or without ISI corrections. PHENIX data are from Refs. [57] (triangles) and [60] (squares).

higher, $\tilde{x}_T = x_T/z_h$, so it reaches values of 0.3–0.5 at RHIC and about 0.4 at LHC ($p_T = 200$ GeV).

Comparison with PHENIX data [56] for neutral pion production in central d-Au collisions is presented in Fig. 11. There is a firm indication in data that the predicted strong nuclear suppression at large x_T is indeed observed. Still, the statistical evidence of the effect needs to be enhanced.

In nuclear collisions the ISI effects are calculated similarly, using the modified parton distribution functions Eq. (36) for nucleons in both colliding nuclei. The resulting complementary suppression reduces $R_{AA}(p_T)$ at large x_T. This is demonstrated in Fig. 12.

If we just repeated the same calculations as done above for the LHC, we would get R_{AA} steeply rising with p_T, as is depicted by the dashed curve. Only the transport coefficient was readjusted to a smaller value $\hat{q}_0 = 1.6$ GeV^2/fm at this energy, compared with $\sqrt{s} = 2.76$ TeV. However the ISI effects and energy conservation impose a sizable additional suppression, as is shown by the solid curve. Apparently this improves the agreement with data.

Keeping $\hat{q}_0$ fixed, we can calculate other observables for gold-gold collisions at $\sqrt{s} = 200$ GeV. Figure 13 presents our results for the suppression of neutral pions at different collision centralities, in comparison with PHENIX data [57].

One can access even larger values of $x_T = 2p_T/\sqrt{s}$, by either increasing p_T or going down in energy. In both cases the effects of ISI should be stronger. Indeed, data for $R_{AA}(p_T)$ in gold-gold collisions at $\sqrt{s} = 62$ GeV plotted in Fig. 14 show a falling, rather than rising, p_T dependence.

Our calculations using Eq. (31) again demonstrate good agreement. Of course, the hot medium properties changed, so we had to readjust the parameter $\hat{q}_0 = 1.2$ GeV^2/fm.

C. Azimuthal anisotropy

Experimental observation of a suppression of high-p_T hadrons escaping from the dense medium means that not the
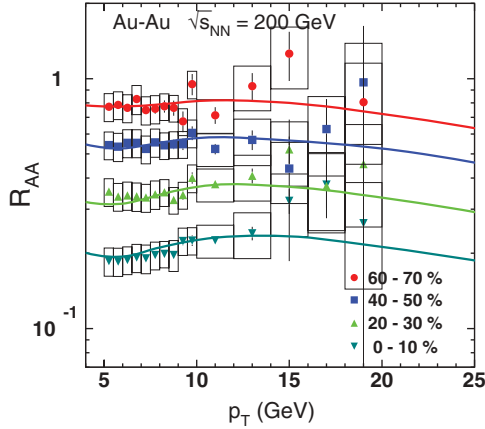
FIG. 13. (Color online) Centrality dependence of the suppression factor $R_{AA}(p_T, b)$ measured in the PHENIX experiment [57] in gold-gold collisions at $\sqrt{s} = 200$ GeV. The intervals of centrality are indicated in the plot.

whole volume of the medium contributes. Independently of the suppression mechanism (except for the contribution of ISI), this means that the longer the path length of propagation in the medium (in two-dimensional transverse plane), the stronger the suppression. Thus, one can conclude that the direction of propagation normally to the medium surface is preferable. For a noncentral collision with an almond shape of the intersection area this should lead to an azimuthal asymmetry of high-p_T hadron production. Although this conclusion should be valid for any mechanism of suppression, the magnitude of the asymmetry is, of course, model dependent.

Our main result for high-p_T hadron suppression, Eq. (31), can be tested by comparison of the predicted azimuthal angle dependence with data. Following data [58], we split the integration over ϕ in (31) into two intervals: (i) $|\phi| > 3\pi/4$ plus $|\phi| < \pi/4$ and (ii) $\pi/4 < |\phi| < 3\pi/4$. These two contributions are called in- and out-of-plane, respectively. As expected, in-plane events are less suppressed compared with out-of-plane, as is depicted by the upper and lower curves in Fig. 15. Our results agree well with ALICE data [58] at $p_T > 6$ GeV and at all measured centralities.
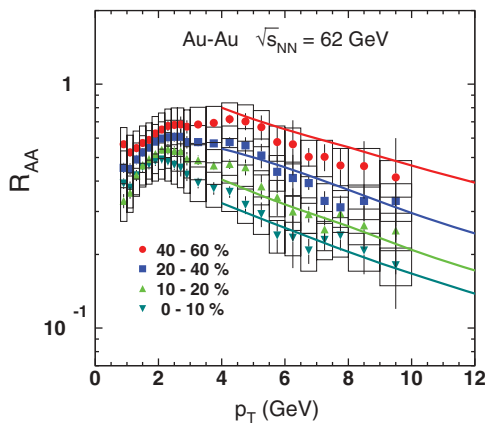
FIG. 14. (Color online) The same as in Fig. 13 but at $\sqrt{s} = 62$ GeV. Data are from Ref. [61].
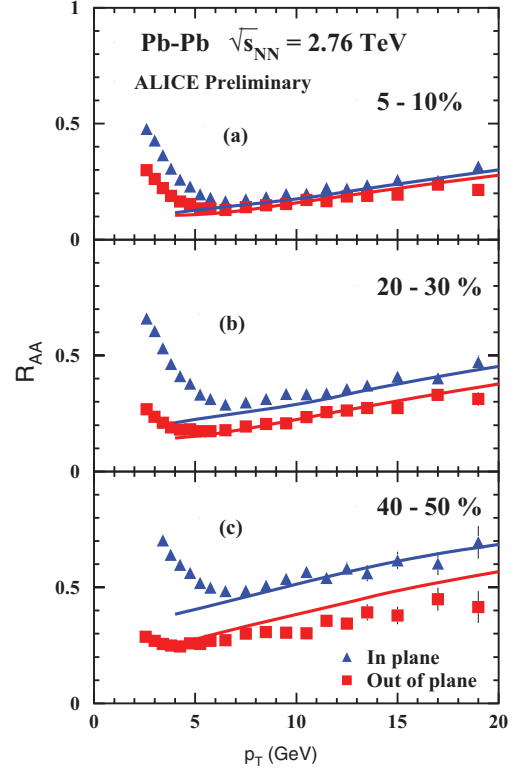
FIG. 15. (Color online) Nuclear factor $R_{AA}(p_T)$ for charge hadrons in lead-lead collisions at $\sqrt{s} = 2.76$ TeV at different centralities indicated on the figure. ALICE data [58] and our calculations with Eq. (31) are divided into two classes: in-plane ($3\pi/4 < |\phi| < \pi$ and $|\phi| < \pi/4$) and out-of-plane ($\pi/4 < |\phi| < 3\pi/4$).

Similar measurements of R_{AA} were performed in the PHENIX experiment for the in- and out-of the-scattering-plane events [57]. The results for centrality 20–30% are plotted in Fig. 16 in comparison with our calculations. Notice that both Figs. 15 and 16 show that the transition from the hydrodynamic to perturbative regimes occur for in-plane events with a delay
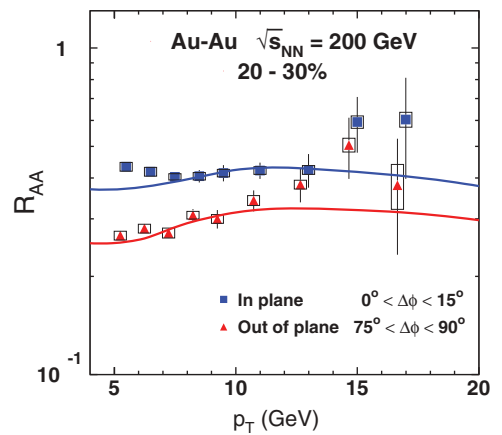
FIG. 16. (Color online) $R_{AA}(p_T)$ for charge hadrons in gold-gold collisions at $\sqrt{s} = 200$ GeV at centralities 0–20%. PHENIX data [57] and our calculations with Eq. (31) are divided into two classes of events: in-plane ($11\pi/12 < |\phi| < \pi$ and $|\phi| < \pi/12$) and out-of-plane ($5\pi/12 < |\phi| < 7\pi/12$).
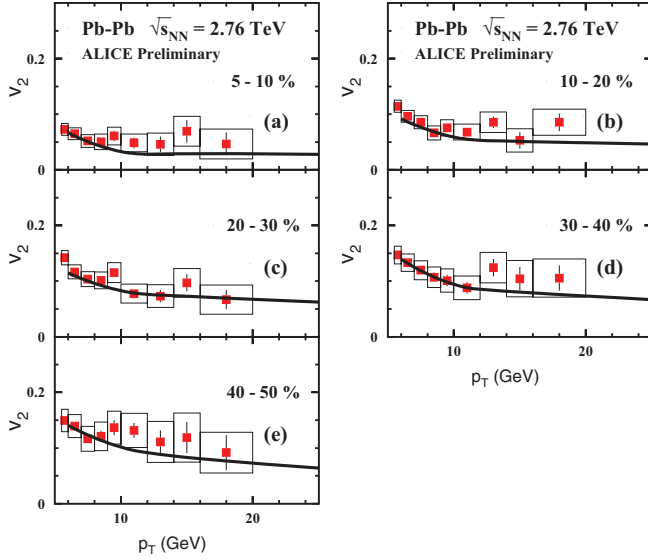
FIG. 17. (Color online) ALICE data [58] for azimuthal anisotropy, v_2, vs p_T for charge hadron production in lead-lead collisions at midrapidity at $\sqrt{s} = 2.76$ TeV and at different centralities indicated in the figure. The curves present the results of calculation with Eq. (37).

FIG. 18. (Color online) The same as in Fig. 17 but displaying data from the CMS experiment [59].

at higher p_T. This is natural, since the hydrodynamic flow is much stronger, and, correspondingly, the cross section is larger.

Usually data on azimuthal asymmetry of particle production are presented in terms of the second moment of the ϕ distribution, $v_2 \equiv \langle \cos(2\phi) \rangle$. We can calculate it with a slight modification of Eq. (31),

$$v_2(p_T, b)$$
$$= \frac{\int d^2\tau\, T_A(\tau) T_B(\vec{b} - \vec{\tau}) \int_0^{2\pi} d\phi \cos(2\phi) |J(\vec{b}, \vec{\tau}, \phi)|^2}{\int d^2\tau\, T_A(\tau) T_B(\vec{b} - \vec{\tau}) \int_0^{2\pi} d\phi |J(\vec{b}, \vec{\tau}, \phi)|^2},$$
$$(37)$$

where

$$J(\vec{b}, \vec{\tau}, \phi) = \int_0^\infty dr\, r\, \Psi_h(r)\, G_{\bar{q}q}(0, 0; l_{\max}, r). \quad (38)$$

We note that the Green function implicitly depends on the impact parameters $\vec{b}$ and $\vec{\tau}$, and on the trajectory of the dipole in the hot matter, and that these dependencies are contained in the functions $\Omega(l_1, l_2)$ and $\Upsilon_i(l_1, l_2)$ in Eq. (30).

In order to compare with data on $v_2(p_T)$, one should integrate the numerator and denominator in (37) over the intervals of impact parameter from $b_{\min}$ to $b_{\max}$, which correspond to the measured intervals of centrality. Our results are compared with ALICE data [58] and with CMS data [59] in Figs. 17 and 18, respectively. In all cases we observe good agreement.

Naturally, as with data on R_{AA}, our pQCD calculations for $v_2(p_T)$ grossly underestimate data at small $p_T \lesssim 6$ GeV. Remarkably, the transition to the pQCD regime occurs for $v_2(p_T)$ at the same p_T as for $R_{AA}(p_T)$. This confirms the presence of two different mechanisms: (i) the hydrodynamic mechanism

of elliptic flow, providing a large and rising with p_T anisotropy $v_2(p_T)$; (ii) the regime of pQCD, having a much smaller azimuthal anisotropy. So it is not accidental that both $R_{AA}(p_T)$ and $v_2(p_T)$ swiftly change their behavior at the same value of p_T.

We also compare our results for the azimuthal anisotropy with RHIC data. Although we included the effects of ISI suppressing R_{AA} at large p_T, these corrections mostly cancel in the ratio [Eq. (37)]. Our calculations agree well with PHENIX data for the azimuthal asymmetry for π^0 production at $\sqrt{s} = 200$ GeV and at midrapidity, as is demonstrated in Fig. 19.
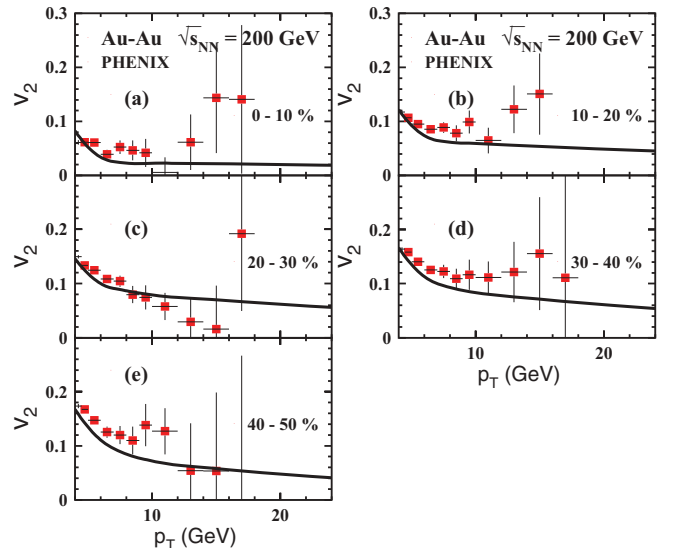
FIG. 19. (Color online) The same as in Fig. 17 but displaying data from the PHENIX experiment [62].

V. SUMMARY AND PROSPECTIVES

This paper attempts a quantitative understanding of experimentally observed strong attenuation of hadrons inclusively produced with large transverse momenta in heavy-ion collisions, based on contemporary models for space-time development of hadronization. The improved quality of data from RHIC and new high-statistics data from LHC make the test of models more challenging and also more decisive. In particular, the popular energy-loss scenario, based on the unjustified assumption of long production length, experiences difficulties explaining the new data. It also fails to explain the data from the HERMES experiment at the Hadron-Electron Ring Accelerator for leading hadron production in semi-inclusive DIS, which provides a sensitive testing ground for in-medium hadronization models.

Here we presented an alternative mechanism of suppression of high-p_T hadrons inclusively produced in heavy-ion collisions. First, we investigated the space-time development of gluon radiation and energy dissipation by a highly virtual parton produced in a high-p_T process. The key point of this consideration is an uniquely high initial virtuality of such a parton, which is of the order of its energy. Thus, increasing the jet energy one simultaneously enhances the hardness of the process, intensifying the dissipation of the energy. For this reason, energy conservation imposes tough constraints on the production length of leading hadrons, which does not rise with p_T but remains short, as is demonstrated in Fig. 5.

It is worth emphasizing that the shortness of the production length is a specific feature of inclusive hadron production. However, formation of a high-p_T jet is characterized by a much longer time scale. Indeed, the convolution Eq. (15) of steeply falling cross section of parton-parton scattering with parton distribution and fragmentation functions strongly enhances the contribution of large z_h, as is demonstrated in Fig. 7. In this case, energy conservation is an important issue and restricts the production length. As for fully reconstructed high-p_T jets, they are characterized by a very different space-time development, and the medium-induced energy loss may be indeed an important source of the observed jet suppression.

With the production of a colorless hadronic state (dipole) the gluon radiation and energy loss cease, and the main reason for suppression of the production rate becomes the survival probability of the prehadron propagating through the dense matter. Apparently, at larger p_T, the expansion of the initially small initial size of the dipole slows down due to Lorentz time dilation. Here the effect of color transparency is at work, and the medium becomes more transparent for more energetic dipoles. A rising nuclear suppression factor $R_{AA}(p_T)$ is indeed observed at LHC, in good accord with the effect of color transparency.

In this paper we performed calculations based on the most strict quantum-mechanical description of space-time development and attenuation of color dipoles propagating through a medium, the path-integral method. We calculated and compared with data the suppression factor $R_{AA}(b)$ for different centralities and energies of collision, ranging from $\sqrt{s} = 62$ GeV to 2.67 TeV. Additional suppression arising from initial-state multiple interactions, important at large x_T or x_L, was also included. The related corrections are found to be important at $x_T \gtrsim 0.1$, where they slow down the rise of R_{AA} and even turn it into a falling p_T dependence. We also calculated the azimuthal anisotropy of hadron production, which reflects the asymmetric shape of the overlap area of the colliding nuclei.

In all cases we reached good agreement with available data from RHIC and LHC at high p_T. The only adjusted parameter, the maximal value of the transport coefficient, Eq. (20), was found to be $\hat{q}_0 = 2$ GeV^2/fm, 1.6 GeV^2/fm and 1.2 GeV^2/fm at $\sqrt{s} = 2.76$ TeV, 200 GeV, and 62 GeV, respectively, for heavy nuclei, lead, and gold.

Our results reproduce quite well the data at $p_T \gtrsim 6$ GeV. However, the observed $R_{AA}(p_T)$ and $v_2(p_T)$ expose quite a different behavior towards smaller p_T, steeply rising and forming a bump. We relate this to an interplay of two mechanisms of hadron production: (i) evaporation of hadrons from the created hot medium controlled by hydrodynamics and (ii) perturbative QCD mechanism of high-p_T production of hadrons, which propagate and attenuate in the hot medium. The abrupt transition between the two mechanisms causes distinct minima in $R_{AA}(p_T)$ and in $v_2(p_T)$, both observed at the same values of p_T. We plan to work on combining the two mechanisms, aiming to describe data in the full range of p_T.

[1] B. Z. Kopeliovich, J. Nemchik, E. Predazzi, and A. Hayashigaki, Nucl. Phys. A **740**, 211 (2004).

[2] B. Z. Kopeliovich, L. I. Lapidus, and A. B. Zamolodchikov, JETP Lett. **33**, 595 (1981) [Pisma Zh. Eksp. Teor. Fiz. **33**, 612 (1981)].

[3] J. Dolejsi, J. Hüfner, and B. Z. Kopeliovich, Phys. Lett. B **312**, 235 (1993).

[4] M. B. Johnson, B. Z. Kopeliovich, and A. V. Tarasov, Phys. Rev. C **63**, 035203 (2001).

[5] B. Z. Kopeliovich, I. K. Potashnikova, and I. Schmidt, Phys. Rev. C **81**, 035204 (2010).

[6] S. Domdey, D. Grunewald, B. Z. Kopeliovich, and H. J. Pirner, Nucl. Phys. A **825**, 200 (2009).

[7] B. Z. Kopeliovich, I. K. Potashnikova, and I. Schmidt, Phys. Rev. C **83**, 021901 (2011).

[8] A. Adare *et al.* (PHENIX Collaboration), Phys. Rev. C **77**, 064907 (2008).

[9] S. Wicks, W. Horowitz, M. Djordjevic, and M. Gyulassy, Nucl. Phys. A **784**, 426 (2007).

[10] B. Z. Kopeliovich, J. Nemchik, I. K. Potashnikova, M. B. Johnson, and I. Schmidt, Phys. Rev. C **72**, 054606 (2005).

[11] A. Casher, H. Neuberger, and S. Nussinov, Phys. Rev. D **20**, 179 (1979).

[12] B. Z. Kopeliovich and F. Niedermayer, Sov. J. Nucl. Phys. **42**, 504 (1985) [Yad. Fiz. **42**, 797 (1985)].

[13] A. Bialas and M. Gyulassy, Nucl. Phys. B **291**, 793 (1987).

[14] A. Accardi and H.-J. Pirner, Nucl. Phys. A **711**, 264 (2002).

[15] B. Z. Kopeliovich, H.-J. Pirner, I. K. Potashnikova, I. Schmidt, and A. V. Tarasov, Phys. Rev. D **77**, 054004 (2008).

[16] B. Z. Kopeliovich, J. Nemchik, and E. Predazzi, in *Future Physics at HERA*, Proceedings of the Workshop 1995/96, edited by G. Ingelman, A. De Roeck and R. Klanner (DESY, Hamburg, 1995/1996), Vol. 2, p. 1038; arXiv:nucl-th/9607036.

[17] B. Z. Kopeliovich, I. K. Potashnikova, and I. Schmidt, Phys. Rev. C **82**, 037901 (2010).

[18] B. Z. Kopeliovich, A. Schäfer, and A. V. Tarasov, Phys. Rev. D **62**, 054022 (2000).

[19] B. Z. Kopeliovich and B. Povh, J. Phys. G **30**, S999 (2004); B. Z. Kopeliovich, B. Povh, and I. A. Schmidt, Nucl. Phys. A **782**, 24 (2007).

[20] J. Ashman *et al.* (European Muon Collaboration), Z. Phys. C **52**, 1 (1991).

[21] A. Airapetian *et al.* (HERMES Collaboration), Eur. Phys. J. C **20**, 479 (2001).

[22] W. K. Brooks and H. Hakobyan, Nucl. Phys. A **830**, 361C (2009).

[23] W. T. Deng and X. N. Wang, Phys. Rev. C **81**, 024902 (2010).

[24] B. Z. Kopeliovich, J. Nemchik, and I. Schmidt, Nucl. Phys. A **782**, 224 (2007).

[25] B. Z. Kopeliovich, H.-J. Pirner, I. K. Potashnikova, and I. Schmidt, Phys. Lett. B **662**, 117 (2008).

[26] J. Binnewies, B. A. Kniehl, and G. Kramer, Phys. Rev. D **52**, 4947 (1995).

[27] B. Z. Kopeliovich, H.-J. Pirner, I. K. Potashnikova, I. Schmidt, A. V. Tarasov, and O. O. Voskresenskaya, Phys. Rev. C **78**, 055204 (2008).

[28] X.-N. Wang, Phys. Rev. C **61**, 064910 (2000).

[29] A. D. Martin, W. J. Stirling, R. S. Thorne, and G. Watt, Eur. Phys. J. C **63**, 189 (2009).

[30] D. de Florian, R. Sassot, and M. Stratmann, Phys. Rev. D **75**, 114010 (2007); **76**, 074033 (2007).

[31] A. Adare *et al.* (Phenix Collaboration), Phys. Rev. D **76**, 051106 (2007).

[32] S. Chatrchyan *et al.* (CMS Collaboration), J. High Energy Phys. 08 (2011) 086; (CMS Collaboration), Eur. Phys. J. C **72**, 1945 (2012).

[33] R. Baier, Y. L. Dokshitzer, S. Peigne, and D. Schiff, Phys. Lett. B **345**, 277 (1995); Nucl. Phys. B **484**, 265 (1997).

[34] X. F. Chen, C. Greiner, E. Wang, X. N. Wang, and Z. Xu, Phys. Rev. C **81**, 064908 (2010).

[35] B. Z. Kopeliovich, Nucl. Phys. A **854**, 187 (2011).

[36] B. Z. Kopeliovich, I. K. Potashnikova, and I. Schmidt, Phys. Rev. C **82**, 024901 (2010).

[37] A. V. Efremov and A. V. Radyushkin, Phys. Lett. B **94**, 245 (1980).

[38] E. L. Berger, Phys. Lett. B **89**, 241 (1980).

[39] K. Aamodt *et al.* (ALICE Collaboration), Phys. Lett. B **696**, 30 (2011).

[40] B. Z. Kopeliovich, A. Schäfer and A. V. Tarasov, Phys. Rev. C **59**, 1609 (1999).

[41] B. Z. Kopeliovich, J. Raufeisen, and A. V. Tarasov, Phys. Lett. B **440**, 151 (1998).

[42] B. G. Zakharov, Phys. At. Nucl. **61**, 838 (1998) [Yad. Fiz. **61**, 924 (1998)].

[43] B. Z. Kopeliovich, J. Nemchik, A. Schäfer, and A. V. Tarasov, Phys. Rev. C **65**, 035201 (2002).

[44] B. Z. Kopeliovich and B. G. Zakharov, Phys. Rev. D **44**, 3466 (1991).

[45] B. Z. Kopeliovich and B. G. Zakharov, Phys. Lett. B **264**, 434 (1991).

[46] B. Z. Kopeliovich, J. Nemchik, N. N. Nikolaev, and B. G. Zakharov, Phys. Lett. B **309**, 179 (1993); **324**, 469 (1994).

[47] B. Abelev *et al.* (The ALICE Collaboration), arXiv:1208.2711 [hep-ex].

[48] Y.-J. Lee (for the CMS Collaboration), J. Phys. G **38**, 124015 (2011).

[49] A. S. Yoon (for the CMS Collaboration), J. Phys. G **38**, 124116 (2011).

[50] Yu. Karpenko (private communication).

[51] B. Z. Kopeliovich and J. Nemchik, J. Phys. G **38**, 043101 (2011).

[52] J. Nemchik, V. Petracek, I. K. Potashnikova, and M. Sumbera, Phys. Rev. C **78**, 025213 (2008).

[53] J. F. Gunion and G. Bertsch, Phys. Rev. D **25**, 746 (1982).

[54] V. A. Abramovsky, V. N. Gribov, and O. V. Kancheli, Yad. Fiz. **18**, 595 (1973) [Sov. J. Nucl. Phys. **18**, 308 (1973)]

[55] B. Z. Kopeliovich, I. K. Potashnikova, and I. Schmidt, Phys. Rev. C **73**, 034901 (2006).

[56] S. S. Adler *et al.* (PHENIX Collaboration), Phys. Rev. Lett. **98**, 172302 (2007).

[57] A. Adare *et al.* (PHENIX Collaboration), arXiv:1208.2254 [nucl-ex].

[58] A. Dobrin (for the ALICE Collaboration), J. Phys. G **38**, 124170 (2011).

[59] S. Chatrchyan *et al.* (CMS Collaboration), arXiv:1204.1850 [nucl-ex].

[60] M. L. Purschke (for the PHENIX Collaboration), J. Phys. G **38**, 124016 (2011).

[61] PHENIX Collaboration, preliminary data posted at www.phenix.bnl.gov/WWW/plots/show_plot.php?editkey=p1118.

[62] A. Adare *et al.* (PHENIX Collaboration), Phys. Rev. Lett. **105**, 142301 (2010).